USE OF RED SUPERGIANT SPECTRAL FEATURES AS AGE INDICATORS IN STARBURST REGIONS

Y. D. MAYYA[1]

Instituto Nacional de Astrofisica, Óptica y Electrónica, Apdo Postal 51 y 216, 72000 Puebla, Pue., México; ydm@inaoep.mx

ABSTRACT

We investigate techniques that can be used to determine ages of starburst regions containing populations beyond their early nebular phase. In particular, we study the strength of the Ca II triplet ($\lambda\lambda$8498, 8542, 8662) and the CO index (2.31–2.40 μm band) using synthetic models as the starburst evolves. For an instantaneous burst of star formation, both of these absorption features remain strongest between 7 and 14 Myr, which corresponds to the red supergiant population. The detailed evolutionary behavior of the starburst is strongly metallicity dependent. Low-metallicity starburst models successfully reproduce the distribution of equivalent widths of the Ca II triplet with age in Large Magellanic Cloud clusters. The clusters in the red supergiant phase strongly favor the stellar evolutionary models incorporating mass-loss rates higher than the standard values. We suggest using of diagrams involving Ca II triplet equivalent width, CO index, and nebular recombination lines to infer the history as well as the age of starburst regions.

Subject headings: galaxies: starburst — Magellanic Clouds — supergiants

1. INTRODUCTION

Detection of Ca II triplet (CaT) lines in a circumnuclear H II region of the starburst galaxy NGC 3310 by Terlevich et al. (1990) offered a new tool to study aging starburst systems. The CaT lines originate in the atmospheres of cool stars with the absorption being the strongest in red supergiants (RSGs). It is known from the stellar evolutionary models at solar metallicity ($Z_\odot = 0.02$) that O stars in the mass range 15–25 $M_\odot$ evolve into RSGs in 7–14 Myr, and hence the detection of the CaT lines in starburst systems is often used to infer the presence of a stellar population of around 10 Myr in age. However, the CaT line equivalent widths of cool giants are nonnegligible, and hence the detection of the triplet lines is not an unambiguous signature of the presence of RSGs.

Bica, Alloin, & Santos (1990) provided a solution to this problem by obtaining the CaT equivalent widths of blue clusters with well-determined turn-off ages in the Large Magellanic Cloud (LMC). They found that only clusters with an age $\sim$10 Myr have CaT equivalent widths greater than 6 Å; the older clusters have values around 4 Å. However, their observed relation has only limited use in estimating the age of starburst regions owing to the fact that the evolutionary history of massive stars, and hence the presence of RSGs, is a strong function of metallicity (Maeder 1991) and that starbursts are found in a wide range of metallic environments. Thus, a quantitative interpretation of the observed equivalent widths in starbursts requires studies of the evolutionary behavior of starbursts at different metallicities. We carry out such a study here with special emphasis on reproducing the observed relations of Bica et al. (1990). We also study the evolutionary behavior of the CO index, which is also sensitive to the population of cool stars, to investigate its use as an age indicator in conjunction with the CaT equivalent widths. As this is one of the first attempts in synthesizing these spectral features (see Leitherer et al. 1996 for a list of on-going attempts), we mainly focus on understanding the basic evolutionary properties and its metallicity dependence. The synthe-

sis technique and the stellar data used are described in § 2. Evolutionary results are presented in § 3 and are discussed from the context of observational data of Bica et al. (1990) for LMC clusters in § 4. The results are discussed from the point of view of age estimations of starburst regions in § 5.

2. SYNTHESIS MODEL AND STELLAR DATA

We use the conventional evolutionary population synthesis technique to compute the starburst-related quantities. The synthesis code we use in the computation is described in detail in Mayya (1995), and the results are compared with other existing codes in Charlot (1996). The major change in the present code is the implementation of the isochrone synthesis technique (Charlot & Bruzual 1991), which has the effect of reducing the noise on the computed quantities. The equivalent width of the CaT absorption lines is computed for an instantaneous burst (IB) of star formation using the formula,

$$\mathrm{EW}_{\mathrm{CaT}}(\mathrm{imf}, t, Z) = \frac{\displaystyle\int_{m_l}^{m_u} L_{\mathrm{CaT}}(m; t; Z) m^{-\alpha}\, dm}{\displaystyle\int_{m_l}^{m_u} L_{8600}(m; t; Z) m^{-\alpha}\, dm},$$

where L_{CaT} is the strength of the CaT absorption feature and L_{8600} is the underlying continuum luminosity per unit Å at the rest wavelength of 8600 Å. The initial mass function (IMF) slope $\alpha = 2.35$ (Salpeter 1955) is chosen with mass limits $m_l = 1$ and $m_u = 100$ in solar units. The CO index is computed by a similar formula with L_{CO} replacing L_{CaT} and the corresponding continuum wavelength being 2.36 μm. It is expressed in magnitude units following the conventional definition. Stellar evolutionary models are used to obtain the spectral type and luminosity class for a star of mass m at evolutionary stage t and metallicity Z. Theoretical model spectra are then assigned to each of these spectral types to enable us to compute the continuum luminosities at 8600 Å and 2.36 μm. The spectra from Kurucz (1992) are used for effective temperatures of stars above 3500 K. At lower temperatures, we use the library

[1] Fellow of the Programa Internacional de Astrofísica Avanzada "Guillermo Haro."

of cool star spectra compiled recently by Lejeune, Cuisinier, & Buser (1996).

We use stellar evolutionary models from Geneva for starburst evolutions at metallicities $Z = 0.001$, 0.008, 0.02, and 0.04. These metallicities encompass a wide range of starburst systems from the metal-poor blue compact galaxies to the metal-rich nuclear starbursts. Geneva models referred as standard (Schaller et al. 1992; Schaerer et al. 1993a, 1993b) assume moderate overshooting of the convective core and use empirical relations for expressing mass-loss rate ($\dot{M}$) for different masses at different metallicities. There are known to be difficulties in explaining all the observables with one set of assumptions (Maeder 1994; Langer & Maeder 1995). Since our interest here is to compute quantities related to RSGs, we looked for those tracks that correctly reproduce the observed ratios of blue to red supergiants (B/R). Meynet (1992) has shown that the standard tracks reproduce the observed B/R at solar metallicity, while at lower metallicity, models with mass-loss rates enhanced by a factor 2.2 reproduce the observed B/R better. Hence we used standard tracks at $Z \geq Z_\odot$ and Meynet et al. (1994) models with enhanced mass-loss rates (by a factor of 2 over standard $\dot{M}$) at lower metallicities.

2.1. *Stellar Data for* Ca II *Triplet and* CO *Index*

The most comprehensive investigation of the dependence of the equivalent width of the CaT with spectral type, luminosity class, and metallicity of stars was carried out by Diaz, Terlevich, & Terlevich (1989; hereafter DTT). They defined the CaT equivalent width, EW(CaT), as the sum of the equivalent widths of two of the brightest lines ($\lambda\lambda 8542$, 8662) and provided an expression relating EW(CaT) with log g and log($Z/Z_\odot$). For metal-rich stars ($Z \geq Z_\odot$), the EW(CaT) increases with decreasing surface gravity, and for supergiants, it increases with increasing metallicity. The dependence on effective temperature was found to be negligible for their sample of cool stars. Independent observational studies by Zhou (1991) and Mallik (1994) support the above findings. Theoretical computations of Jorgensen, Carlsson, & Johnson (1992; hereafter JCJ) successfully reproduced all the basic trends established by DTT. However, they found that the theoretically based relations involving higher order terms in log g are better fits to the observed data than the linear relation of DTT, which underestimates the EW(CaT) by ~2–5 Å in metal-rich red supergiants. Hence, we use the JCJ relation for $Z \geq Z_\odot$ and the DTT relation at lower metallicities.

Data on the CO band are not as complete as that for the CaT. The best published data set so far is that of Kleinmann & Hall (1986) for a sample of 26 stars covering a wide range of spectral type and luminosity classes, but at solar metallicity only. Doyon, Joseph, & Wright (1994) defined the CO index based on the spectra in the above sample and obtained relations for the CO index as a function of effective temperature for dwarfs, giants, and supergiants separately. These make up the basis for our computations. The above defined index (CO_{sp}) is related to the photometrically measured index (CO_{ph}; Frogel et al. 1978) by $CO_{sp} = 1.46 \, CO_{ph} - 0.02$.

3. SYNTHETIC RESULTS FOR Ca II TRIPLET AND CO INDEX

The evolutionary behavior of the EW(CaT) at the four metallicities is shown in Figure 1a. The following important stages can be recognized during the evolution of solar metal-
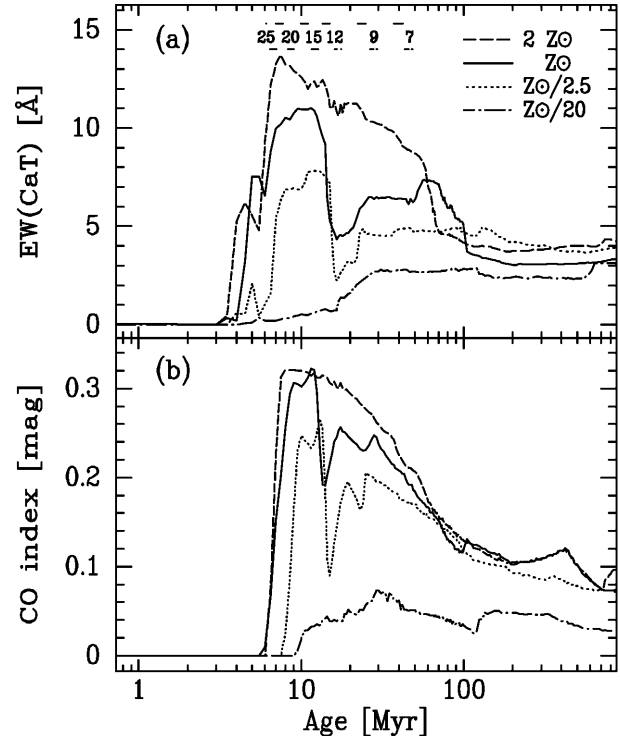

FIG. 1.—Evolution of (*a*) the equivalent width of the Ca II triplet and (*b*) the CO index for an instantaneous burst of star formation for the assumed Salpeter initial mass function, at the four chosen metallicities. Supergiant phases of massive stars at $2Z_\odot$ (*top*) and $Z_\odot$ metallicities are shown by the parallel horizontal bars, with the numbers in the middle denoting the stellar masses in $M_\odot$.

licity starbursts.

Stage 1.— EW(CaT) rises to detectable levels in starbursts, 5 Myr after the onset of the IB, reaching the highest values of ~11 Å between 7 and 14 Myr.

Stage 2.—The EW abruptly drops to around 5 Å at ~15 Myr, remaining at these low values up to around 20 Myr.

Stage 3.—The EW rises again above 6.5 Å at 25 Myr, showing a secondary peak at 60 Myr.

Stage 4.—The EW attains an asymptotic value of around 3 Å after 100 Myr.

The evolutionary behavior at $Z = Z_\odot/2.5$ is qualitatively similar to that of $Z_\odot$ models. However, the peak values, as well as the contrast between Stages 1, 3, and 4 above, are lower. The trend of decreasing contrast continues at lower metallicity, which results in steady values of around 2 Å throughout Stages 3 and 4 for the $Z_\odot/20$ model. The most significant feature during the evolution of low-metallicity starbursts is the absence of the primary peak at 10 Myr (Stage 1). At intermediate metallicities ($Z_\odot/5$; not plotted), the 10 Myr peak is present (2 Å) but at values lower than at Stage 3 (5 Å). At higher than solar metallicities, Stage 2 is missing, which results in a smooth decrease of the EW from Stage 1 to the end of Stage 3.

Stages 1–4 as well as their dependence on metallicity can be understood by identifying the individual phases, which contribute significantly to the EW(CaT), during stellar evolution. The cool giant and supergiant phases of different stellar masses are depicted in Figure 1 by horizontal bars at the upper part of the diagram. The primary peak at ~10 Myr at all the metallicities

is directly related to the cool RSG population of progenitor masses between 15–25 $M_\odot$. The supergiants at the lowest metallicity we have considered spend most of their post–main-sequence evolution as blue supergiants and hence fail to show the peak at 10 Myr.

Note that the horizontal bars depicting the cool giant and supergiant phases have a discontinuity for stars of mass ≤ 12 $M_\odot$ at solar metallicity. This break is due to the qualitatively different post–main-sequence evolution of 12 $M_\odot$ and lower mass stars for $Z \leq Z_\odot$. These stars go through the well-established "blue loop" in the Hertzsprung-Russell diagram during the core helium burning phase, returning to the redder phase only at the end of core helium burning. Thus, there is a sudden reduction in the number of RSGs in the starburst, which explains Stage 2. "Blue loops" during core helium burning is a common property of stellar evolutionary models for $Z \leq Z_\odot$, and hence the $Z_\odot/2.5$ model behaves qualitatively similarly to the $Z_\odot$ model. On the other hand, "blue loops" are absent for higher metallicity models, and hence there is a smooth transition from the RSG-dominated phase to the red giant– and asymptotic giant branch–dominated phases at $Z = 2Z_\odot$.

Successively lower mass stars spend a lesser fraction of their post–main-sequence lifetime in "blue loops," which results in the accumulation of red giant and asymptotic giant branch stars, leading to the secondary peak at 60 Myr for $Z_\odot$ models. The adopted scaling between mass-loss rate and metallicity and also the corresponding phases for a star of given mass being warmer at lower metallicities result in the net decrease of the number of stars contributing to CaT absorption at lower metallicities. This is the reason for lower peak values as well as lesser contrast between different stages at lower metallicities. After 100 Myr, the EW(CaT) is controlled by the cool giant and dwarf stars of mass <5 $M_\odot$.

Evolution of the CO_{sp} index is shown in Figure 1b. Note that the metallicity dependence in this plot arises only because of the dependence of stellar evolution on metallicity; there is no data set on its dependence on line formation. The evolutionary behavior, as well as its dependence on metallicity, can be understood by the same physical phenomenon as that for the EW(CaT). However, the following quantitative differences in the four stages are noteworthy.

Stage 1.—The RSG peak is narrower for $Z \leq Z_\odot$ (8–12 Myr).

Stage 2.—The CO index rises faster after the drop following the "blue loop" phase.

Stage 3.—The secondary maximum occurs at 20–30 Myr. There is a smooth decrease from this epoch onward.

Stage 4.—The CO index does not reach asymptotic values beyond 100 Myr.

These differences arise, first, owing to a stronger dependence of the CO index on the effective temperature and second, owing to the same stars contributing to the continuum as well as the CO absorption strength. The CO index of the starburst is essentially that of the most luminous cool star, as these cool stars contribute both to the line depth as well as the continuum. In contrast, the continuum at CaT has a significant contribution from hotter stars, and hence the EW(CaT) evolves differently than that of the CO index.

4. COMPARISON WITH LMC CLUSTERS

The blue clusters of the LMC provide a unique opportunity of checking the evolutionary results discussed above before these results can be used to derive ages of starburst systems. The special advantage of these clusters is the availability of well-determined turn-off ages. As discussed earlier, Bica et al. (1990) had obtained the EW(CaT) for each cluster, treating each cluster as a single entity. Bica et al. also compiled the CO indices and broadband colors for each of these clusters, which are ideal for comparison with our results. We superimpose our model results on these observed data in Figure 2. The strength of the fainter $\lambda 8498$ line has been subtracted from the Bica et al. value to covert the observed values to the more commonly used definition of DTT. Photometrically derived CO indices are converted into CO_{sp} using the relation given in § 2.1. The available $J - K$ and $B - V$ colors are also plotted in the last two panels. The solid and dashed lines correspond to models using enhanced and standard mass-loss rates respectively, both at $Z_\odot/2.5$ metallicity.

The ages of the clusters with the highest EW(CaT), CO index and $J - K$ color agree very well with the RSG-dominated bump (Stage 1) in our model. The absolute values of the RSG peak with stellar evolution incorporating standard mass-loss rate are too low to account for the observations, which confirms the underestimation of RSGs in these models. Using enhanced mass-loss rate models correctly reproduces the EW(CaT) and $J - K$ color. The observed CO index is still higher by around 0.08 mag, which might be caused by errors introduced in converting the photometrically observed indices to spectroscopic indices. The larger scatter in this plot compared to the other plots also suggests larger errors in the observed CO indices. Thus, we conclude that the stellar evolution with enhanced mass-loss rates, and not the standard, is a better representation of the observed values in LMC.

Older clusters have EW(CaT), CO index, and $J - K$ as predicted for Stage 3 in our model. However, only the lower boundary of the observed $B - V$ colors agrees with the model predictions for Stage 3 with the majority of the clusters having colors around 0.1 mag redder. A similar trend is also seen in $U - B$ colors (not plotted), which is most likely due to the internal reddening in the clusters. It is interesting to note that the observed $B - V$ (and also $U - B$) colors during the RSG phase are bluer than the predictions of the enhanced mass loss rate models.

5. DISCUSSION AND OUTLOOK

Having studied the evolutionary behavior of the CaT equivalent width and the CO index, we now discuss their use in estimating ages of starburst regions from observed data. Diagrams involving dimensionless quantities play an important role in this direction. Most of such attempts hitherto are based on the presence of massive O stars or Wolf-Rayet stars and hence are applicable only as long as the starburst nebula is traceable. The end of nebular phase coincides with the beginning of the RSG phase for an IB, as the ionization is mostly controlled by stars having masses higher than the progenitors of the RSGs (~ 30 $M_\odot$). This is illustrated in the top panel of Figure 3. It can be seen that by the time the EW(CaT) attains the peak value, the Hα emission equivalent width has dropped below the detection limit. We investigated various diagrams involving EW(CaT), CO index, and colors for the four metallicities and found the EW(CaT)-CO index
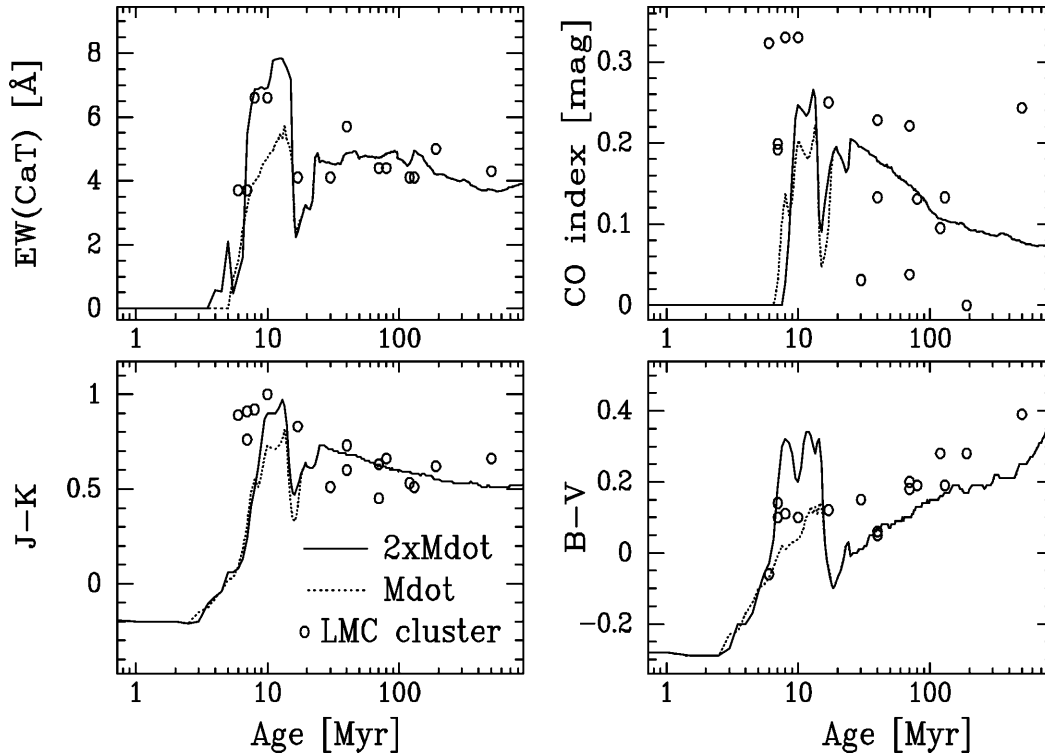
FIG. 2.—Comparison of the computed quantities at $Z = Z_\odot/2.5$ with the observational data of Bica et al. (1990) for the LMC clusters. Stellar evolutionary models incorporating twice the standard mass-loss rate (*solid line*) reproduce the observed characteristics better. IB model with Salpeter IMF is used.
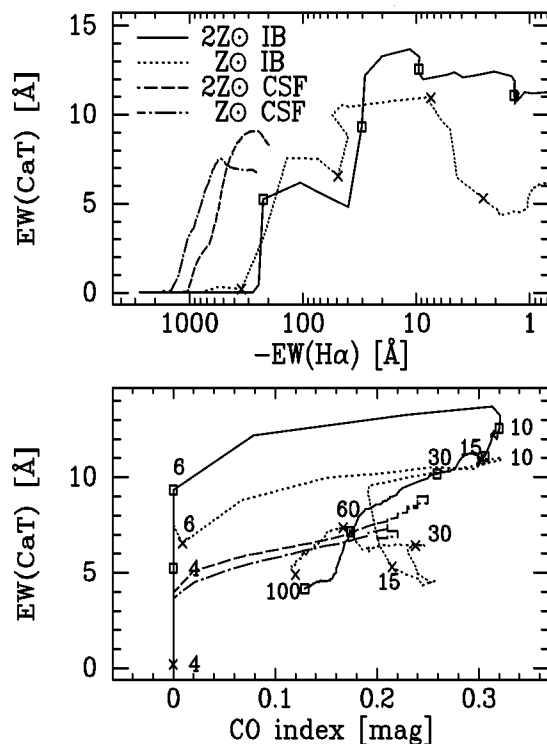

FIG. 3.—Dimensionless diagrams involving observational quantities for $Z = Z_\odot$ and $Z = 2Z_\odot$ models with instantaneous burst and continuous star formation (CSF) at a constant rate. The numbers next to tick marks are starburst ages in Myr. For the CSF, model values stabilize at ~15 Myr.

plane to be the best suited for the purpose of age determination. The loci of IB and continuous star formation (CSF) models at $Z = 2Z_\odot$ and $Z_\odot$ are shown in Figure 3. Selected ages in Myr are indicated along the locus in this plot.

In the EW(CaT) versus EW(Hα) plot, the IB and CSF models follow quite different tracks and hence can be most effectively used to infer the history of star formation; e.g., regions with detectable EW(CaT) and emission EW(Hα) greater than 300 Å can be described only by CSF. For CSF models, asymptotic values are reached in ~15 Myr. Once the history of star formation is known, the EW(CaT) versus CO index plot can be used to derive accurate ages of starburst regions. The ambiguity in the estimated age increases with decreasing metallicity for IB models, with the result that similar plots for $Z < Z_\odot$ have limited use. However, our models give a definite upper limit for low-metallicity systems. The blue compact galaxies with $Z < Z_\odot/5$ are not expected to have EW(CaT) and CO index values above 5 Å and 0.1 dex, respectively. These values are insensitive to mass limits as long as $m_u \geq 30\ M_\odot$ and $m_l \leq 3\ M_\odot$ and are only weakly sensitive to the IMF slope.

Before we end, we point out the limitations of the present work and discuss where further improvements are necessary. Our main purpose in this work was to investigate the important stages during evolution of EW(CaT) and CO index in starburst regions and their metallicity dependence, and accordingly we kept the starburst model at the simplest level. Observed values in nuclear starbursts may have some contribution from the bulge light (see, e.g., García-Vargas et al. 1997), and hence using Figure 3 for nuclear starbursts may require a separate treatment of the bulge. However, Figure 3 is directly applicable for high-metallicity giant H II regions in

disks of galaxies. Our next step is to study the dilution of the computed quantities as a function of fractional contribution of the bulge light, which will enable direct comparison with observed data of starburst nuclei.

REFERENCES

Bica, E., Alloin, D., & Santos, J. F. C., Jr. 1990, A&A, 235, 103
Charlot, S. 1996, in ASP Conf. Proc. 98, From Stars to Galaxies, ed. C. Leitherer, Fritze–v. Alvensleben, & J. Huchra (San Francisco: ASP), 275
Charlot, S., & Bruzual, A. 1991, ApJ, 367, 126
Diaz, A. I., Terlevich, E., & Terlevich, R. 1989, MNRAS, 239, 325 (DTT)
Doyon, R., Joseph, R. D., & Wright, G. S. 1994, ApJ, 421, 101
Frogel, J. A., Persson, S. E., Aaronson, M., & Matthews, K. 1978, ApJ, 220, 75
García-Vargas, M. L., et al. 1997, ApJ, 478, 112
Jorgensen, U. G., Carlsson, M., & Johnson, H. R. 1992, A&A, 254, 258 (JCJ)
Kleinmann, S. G., & Hall, D. N. B. 1986, ApJS, 62, 501
Kurucz, R. L. 1992, in IAU Symp. 149, Stellar Populations of Galaxies, ed. B. Barbuy & A. Renzini (New York: Kluwer), 225
Langer, N., & Maeder, A. 1995, A&A, 295, 685
Leitherer, C., et al. 1996, PASP, 108, 996
Lejeune, T., Cuisinier, F., & Buser, R. 1996, in ASP Conf. Proc. 98, From Stars to Galaxies, ed. C. Leitherer, U. Fritze-v. Alvensleben, & J. Huchra (San Francisco: ASP), 94

Maeder, A. 1991, A&A, 242, 93
———. 1994, Space Sci. Rev., 66, 349
Mallik, S. V. 1994, A&AS, 103, 279
Mayya, Y. D. 1995, AJ, 109, 2503
Meynet, G. 1992, in The Feedback of Chemical Evolution on Stellar Content of Galaxies, ed. D. Alloin & G. Skasinska (Paris: Obs. Paris), 40
Meynet, G., Maeder, A., Schaller, G., Schaerer, D., & Charbonnel, C. 1994, A&AS, 103, 97
Salpeter, E. E. 1955, ApJ, 121, 161
Schaerer, D., Charbonnel, C., Meynet, G., Maeder, A., & Schaller, G. 1993a, A&AS, 102, 339
Schaerer, D., Meynet, G., Maeder, A., & Schaller, G. 1993b, A&AS, 98, 523
Schaller, G., Schaerer, D., Meynet, G., & Maeder, A. 1992, A&AS, 96, 269
Terlevich, E., Diaz, A. I., Pastoriza, M. G., Terlevich, R., & Dottori, H. 1990, MNRAS, 242, 48P
Zhou, X. 1991, A&A, 248, 367